Polariton optics of semiconductor photonic dots: weak and strong coupling limits

2004 J. Phys.: Condens. Matter 16 S3703

(http://iopscience.iop.org/0953-8984/16/35/012)

INSTITUTE OF PHYSICS PUBLISHING JOURNAL OF PHYSICS: CONDENSED MATTER

J. Phys.: Condens. Matter **16** (2004) S3703–S3719 PII: S0953-8984(04)83273-9

Polariton optics of semiconductor photonic dots: weak and strong coupling limits

N I Nikolaev, A Smith and A L Ivanov

School of Physics and Astronomy, Cardiff University, PB 913, Cardiff CF24 3YB, UK

Received 6 July 2004
Published 20 August 2004
Online at stacks.iop.org/JPhysCM/16/S3703
doi:10.1088/0953-8984/16/35/012

Abstract

We develop coherent optics of dipole-active, dispersionless excitons in spherical semiconductor photonic dots (PDs). In the absence of any incoherent scattering, both the strong and weak coupling regimes can intrinsically be realized simply by changing the parameters of the dot and surrounding medium. A criterion, which attributes the transition between these two regimes to a discrete topological change of the relevant dispersion curves, is found and approximated by an analytic expression. The transition depends upon the intrinsic radiative lifetime of the PD photon eigenstates, i.e. it is determined by the parameters of the structure (the oscillator strength of the exciton–photon interaction, PD radius and the ratio of the background dielectric constants inside and outside of the dot). We propose the use of high-precision modulation spectroscopy in order to visualize the above 'phase' transition between a well-developed polariton picture (the strong coupling regime) and weakly-interacting exciton and PD photon states (the weak coupling regime). It is shown that the radiative decay of optically dressed PD excitons, coherently distributed among the relevant PD eigenstates, is non-monotonous against the dot radius a: a size-dependent increase of the effective oscillator strength at small a saturates at $a \sim \lambda$, and with a increasing further towards $a \gg \lambda$ the optical lifetime of excitons starts to increase proportionally to a, reflecting the ballistic escape of nearly bulk polaritons from the PD. The numerical simulations are scaled to dispersionless excitons in PDs fabricated from cyanine dye J aggregates.

(Some figures in this article are in colour only in the electronic version)

1. Introduction

The study of three-dimensional light-trapping has attracted considerable attention in recent years. A cavity built with dimensions of the order of the wavelength of light, λ, such as a spherical photonic dot (PD), serves to form an optical resonator, which has been shown to provide insight into questions of fundamental physics as well as promising many novel

applications (see for example [1, 2] and many references therein). One of the most attractive applications is the coupling of light modes between a PD and a semiconductor quantum dot (QD—a structure with dimensions much less than the wavelength of light) embedded inside of it [3, 4].

Pioneering work on the scattering of light from spheres with constant dielectric permittivity was done by Mie [5] at the beginning of the last century, and the conjugate eigen-mode problem was later discussed by Stratton [6] (see also [7]). Polariton modes [8, 9] in an ionic crystal sphere were investigated by Fuchs and Kliewer [10], who showed that every radiative polariton mode contributes a Lorentzian peak to the cross section for scattering, extinction and absorption, from the sphere. Polariton modes in optical and electronic confinement structures such as microcrystallites [11–13] and quantum dots [14, 15] have been studied, where the radius of the structure is so small that features in the polariton dispersion arise mainly from size quantization of the excitonic energy. Ajiki *et al* have recently presented polariton optics in a weak exciton–photon interaction regime for large-size photonic dots [16, 17] using a microscopic non-local theory [18].

The nature of a polariton mode depends upon the strength of exciton–photon interaction (oscillator strength) in the material, and how close the photon frequency is to the excitonic resonance [8, 9, 19, 20]. In materials with a high oscillator strength the polariton modes are formed from a hybridization of a photon mode and the exciton, and this is called the *strong coupling regime*. In the opposite case, the *weak coupling regime*, materials with low oscillator strengths exhibit polariton modes which are only slightly perturbed from the non-interacting photon and exciton dispersions. Tait has investigated the transition between these two regimes for polaritons in bulk semiconductors [19]: his theory uses the incoherent scattering rate, γ_x, as a control parameter, so that by changing temperature, and hence γ_x, one realizes the two limits. In contrast we present a model for the coherent polariton optics of dispersionless excitons in a single spherical PD, which assumes that the incoherent scattering rate is small and can be neglected, $\gamma_x = 0$. We demonstrate that the transition between the weak and strong coupling regimes occurs due to changes in the intrinsic optical decay of PD excitons, γ_r, via changes in the system parameters.

In this paper we develop the polariton optics of mid-size (a few photonic wavelengths) semiconductor PDs, and in particular study a transition between the weak and strong coupling regimes of exciton–photon interaction. Our results can be directly applied to spherical PDs fabricated from a cyanine dye J aggregate material. The dispersionless Frenkel excitons in these organic semiconductors have been studied recently [21].

In section 2 we review the dispersion equations for polariton modes of spherical PDs. We introduce an entirely optically coherent picture (no incoherent damping) and proceed to classify the polariton modes for any strength of PD-exciton–photon interaction. In section 3 we derive analytical approximations of the radiative lifetime of the polariton branches as a function of the photonic dot radius, and use the coherent distribution of excitons to determine the total radiative lifetime. In section 4 the topology of the polariton dispersion curves is shown to alter from the weak-coupling regime to the strong-coupling regime as the parameters of the system are changed. We derive an analytic approximation to describe the critical values at which this discrete transition occurs, and illustrate how it might be observed using high-precision modulation spectroscopy. Finally section 5 summarizes our conclusions.

2. Classification of PD polaritons

The set of macroscopic polariton equations for the resonantly interacting light field **E** and excitonic polarization **P** is given by [9]

$$\frac{\varepsilon_{\rm b}}{c^2}\frac{\partial^2}{\partial t^2}\mathbf{E}(\mathbf{r},t)+\mathrm{curl}\,\mathrm{curl}\,\mathbf{E}(\mathbf{r},t)=-\frac{1}{\varepsilon_0 c^2}\frac{\partial^2}{\partial t^2}\mathbf{P}(\mathbf{r},t),$$
$$\left[\frac{\partial^2}{\partial t^2}+\gamma_x\frac{\partial}{\partial t}+\omega_T^2-\frac{\hbar\omega_T}{M_x}\nabla^2\right]\mathbf{P}(\mathbf{r},t)=\varepsilon_0\varepsilon_{\rm b}\omega_{\rm p}^2\mathbf{E}(\mathbf{r},t). \tag{1}$$

Here $\varepsilon_{\rm b}$ is the high frequency background dielectric constant of the optically isotropic semiconductor, $\omega_{\rm p}$ is the polariton Rabi frequency, $\hbar\omega_T$ is the exciton energy, M_x is the exciton translational mass, and γ_x is the rate of incoherent scattering of excitons. For Frenkel excitons in isotropic crystals, M_x can be large so that the spatial dispersion associated with excitons is negligible. In this case, for the transverse ($\mathrm{div}\,\mathbf{E}=0$) polariton waves of frequency ω and wavevector $\mathbf{k}$ in bulk materials, equations (1) yield

$$\frac{k^2c^2}{\omega^2}=\varepsilon(\omega)=\varepsilon_{\rm b}\left[1+\frac{\omega_{\rm p}^2}{\omega_T^2-{\rm i}\omega\gamma_x-\omega^2}\right], \tag{2}$$

while the longitudinal mode ($\mathrm{curl}\,\mathbf{E}=0$) is characterized by $\omega_L=\sqrt{\omega_T^2+\omega_{\rm p}^2}$.

For a spherical photonic dot, the PD polariton (quasi-) eigenstates are the solutions of equations (1), written in spherical co-ordinates and satisfying the boundary conditions for the light field. Two Maxwellian boundary conditions refer to the spherical surface at $r=a$ (a is the PD radius) and require the continuous behaviour of the tangential components of the electric, $\mathbf{E}_\tau$, and magnetic, $\mathbf{H}_\tau$, fields. The third boundary condition requires the light field at $r\to\infty$ to have an outgoing part only (no incoming field). It is the third boundary condition which is responsible for the complex PD polariton eigen-frequencies, $\omega=\omega^{\rm pol}$, even if the incoherent scattering of excitons is neglected, i.e. $\gamma_x=0$. As we demonstrate below, for the photonic dots we are dealing with, the optical lifetime of PD photons is short—in a sub-picosecond time scale—so that the 'optical evaporation' of PD polaritons is rather effective, and $\mathrm{Im}\{\omega^{\rm pol}\}$ is usually much larger than γ_x. Thus, in further analysis we neglect the γ_x-terms in equations (1) and (2).

For the transverse light field ($\mathrm{div}\,\mathbf{E}=0$), the PD polariton dispersion equations are given by [10, 22]

$$j_l(k_1a)H_l^{(1)\prime}(k_2a)-h_l^{(1)}(k_2a)J_l'(k_1a)=0, \tag{3}$$

for the TE modes, and

$$\varepsilon j_l(k_1a)H_l^{(1)\prime}(k_2a)-\varepsilon_{\rm d}h_l^{(1)}(k_2a)J_l'(k_1a)=0, \tag{4}$$

for the TM modes. Here $J_l(z)=zj_l(z)$ and $H_l^{(1)}(z)=zh_l^{(1)}(z)$, where $j_l(z)$ and $h_l(z)$ are spherical Bessel and Hankel functions of the first kind; $k_1=k_1(\omega)=\omega\sqrt{\varepsilon}/c$, where $\varepsilon=\varepsilon(\omega)$ is given by equation (2); $k_2=k_2(\omega)=\omega\sqrt{\varepsilon_{\rm d}}/c$, where $\varepsilon_{\rm d}$ is the constant dielectric permittivity of the material surrounding the sphere. The dispersion equations (3) and (4) are similar to those discussed in [6] for PDs without excitonic resonance. Note that the TE and TM modes, given by equations (3) and (4), have a longitudinal component without violating the $\mathrm{div}\,\mathbf{E}=0$ condition. The subscript l refers to the angular momentum of the modes, which are frequency degenerate with respect to the momentum projection quantum number, m.

In this work only modes with the lowest possible angular momentum number, $l=1$, [23] (TE_1 and TM_1) will be considered. In the following analysis we will frequently use the dimensionless, normalized variables: frequency $\tilde\omega=\omega/\omega_T$, Rabi frequency $\tilde\omega_{\rm p}=\omega_{\rm p}/\omega_T$, PD radius $\tilde a=\sqrt{\varepsilon_{\rm b}}\omega_T a/c$, and dielectric permittivity $\tilde\varepsilon=\varepsilon_{\rm d}/\varepsilon_{\rm b}$.

For $l=1$, the PD polariton dispersion equations (3) and (4) reduce to

$$k_1a=\arctan\left[\frac{k_1k_2^2a}{{\rm i}k_1^2k_2a-k_1^2+k_2^2}\right]+n\pi, \tag{5}$$

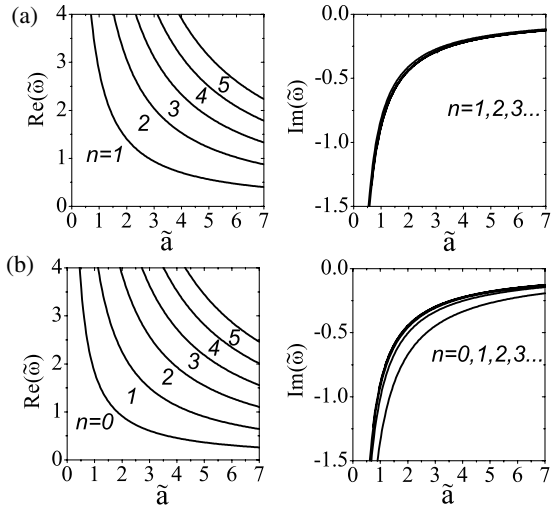

Figure 1. The dependence of the frequency of the photon modes on the PD radius for (a) TE_1 modes and (b) TM_1 modes; $\tilde{\omega}_p = 0$ and $\tilde{\varepsilon} = 0.5$.

for the TE_1 modes, and

$$k_1 a = \arctan\left[\frac{-ik_1 a[k_1^2 k_2^2 a^2 + (1 - ik_2 a)(k_2^2 - k_1^2)]}{k_1^2 k_2^3 a^3 + (k_2 a + i)(k_1^2 - k_2^2)}\right] + n\pi, \tag{6}$$

for the TM_1 modes. Here $n = 0, 1, 2, \ldots$ is the energy (radial) quantum number.

The photon eigen-frequencies $\tilde{\omega}_n^0$ against the dot radius $\tilde{a}$, calculated with equations (5) and (6) for $\tilde{\varepsilon} = 1/2$ and $\tilde{\omega}_p = 0$ (no excitonic resonance), are plotted in figure 1. For a given PD radius $\tilde{a}$, the photon n-eigen-harmonics can be interpreted in terms of the interference pattern of the order n, which arises due to the partial reflection of the light field at the PD spherical boundary. The contrast of the interference pattern as well as the radiative lifetime of PD photons, $\tau_n = -1/(2\ \mathrm{Im}\{\omega_n^0\})$, strongly depend upon $\tilde{\varepsilon}$, i.e. upon the jump of the dielectric constant from ε_b at $r \leqslant a$ to ε_d at $r > a$.

In the presence of the dipole-active dispersionless exciton state with frequency $\tilde{\omega}_T = 1$, the PD photon frequencies $\tilde{\omega}_n^0$ no longer characterize the true eigenstates, due to the resonant exciton–photon interaction. Within the completely coherent picture of exciton–photon coupling ($\gamma_x = 0$), the uncoupled photon and exciton states are replaced by PD polariton eigenwaves. In this case the dispersion equations (3) and (4) yield the PD polariton eigen-frequencies $\tilde{\omega} = \tilde{\omega}_n^{\mathrm{pol}}(\tilde{a})$. By analysing the way (topology) the PD polariton dispersion arises from the initial exciton and photon terms, $\tilde{\omega}_T(\tilde{a}) = 1$ and $\tilde{\omega}_n^0(\tilde{a})$, and develops with increasing Rabi frequency $\tilde{\omega}_p$, we distinguish two limits of exciton–photon interaction in PDs: the weak (small $\tilde{\omega}_p$) and strong (large $\tilde{\omega}_p$) coupling regimes.

The weak coupling regime. The PD polariton dispersion $\tilde{\omega} = \tilde{\omega}_n^{\mathrm{pol}}(\tilde{a})$, calculated with equation (5), is illustrated in figure 2 for the weak coupling limit. The resonant crossover between the PD photon and exciton eigen-frequencies, which occurs when $\mathrm{Re}\{\tilde{\omega}_n^0(\tilde{a} = \tilde{a}_n)\} = 1$, does not result in any drastic, 'topological' changes of the PD polariton dispersion curves. In other words, the PD polariton dispersion curves can naturally be classified in terms of the photon-like, $\tilde{\omega}_n^{\mathrm{pol}} = \tilde{\omega}_n^{\gamma}$ (thin blue lines in figure 2), and exciton-like $\tilde{\omega}_n^{\mathrm{pol}} = \tilde{\omega}_n^{x}$ (thick red curves in figure 2) polariton branches: $\tilde{\omega}_n^{\gamma}(\tilde{a})$ and $\tilde{\omega}_n^{x}(\tilde{a})$ are nearly identical to $\tilde{\omega}_n^0(\tilde{a})$ and $\tilde{\omega}_T(\tilde{a}) = 1$, respectively. The weak resonant exciton–photon coupling does not lead to the

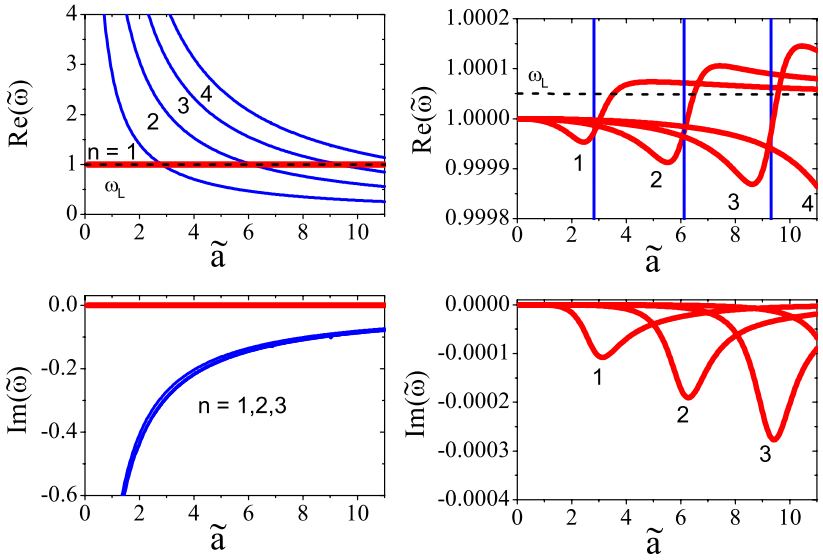

Figure 2. The PD polariton eigen-frequencies $\tilde{\omega} = \tilde{\omega}^{\rm pol}_{n=1,2,3...}(\tilde{a})$ for the TE_1 mode in the weak coupling regime; $\tilde{\omega}_p = 0.01$ and $\tilde{\varepsilon} = 0.5$. The photon-like (exciton-like) dispersion curves are shown by thin blue (thick red) solid curves. In the right-hand-side figures, the polariton dispersion curves are plotted on a magnified scale to illustrate the fine structure of the exciton-like modes (the frequency band is very close to $\tilde{\omega}_T = 1$).

interconnection between the PD photon-like and exciton-like branches in the vicinity of $\tilde{a}_n$, where the most significant change of the dispersion curves takes place. Thus the photon-like (exciton-like) polariton dispersion branch can be interpreted as $\tilde{\omega}^0_n(\tilde{a})$ ($\tilde{\omega}_T(\tilde{a})$), slightly deformed near $\tilde{a} = \tilde{a}_n$ (see the right-hand-side plots of figure 2). The condition $\mathrm{Re}\{\tilde{\omega}^0_n(\tilde{a})\} = 1$ yields

$$\tilde{a}_n \simeq \begin{cases} (n + 1/2)\,\pi, (n = 0, 1, 2, \ldots) & \text{for } \mathrm{TM}_1\ (\tilde{\varepsilon} < 1) \quad \text{and} \quad \mathrm{TE}_1\ (\tilde{\varepsilon} > 1), \\ n\pi, (n = 1, 2, \ldots) & \text{for } \mathrm{TM}_1\ (\tilde{\varepsilon} > 1) \quad \text{and} \quad \mathrm{TE}_1\ (\tilde{\varepsilon} < 1). \end{cases} \tag{7}$$

For the PD radius $\tilde{a} \simeq \tilde{a}_n$, a negative imaginary part of the exciton-like n-polariton eigen-harmonics, $\mathrm{Im}\{\tilde{\omega}^x_n\}$, has a local minimum (see the bottom right-hand-side plot of figure 2). In this case the excitonic state resonates with the PD photon n-eigen-harmonics and can more effectively decay into the bulk photon modes. The electric and magnetic eigen-fields of the photon-like TE_1 polaritons are plotted in figure 3 for the radial energy states $n = 1$, 2 and 3.

The strong coupling regime. In figure 4 we plot the PD polariton dispersion calculated with equation (5) for the strong coupling limit. In this case one has a well-developed polariton effect: a drastic change, so-called anti-crossing, of the initial PD photon and exciton terms occurs near $\tilde{a} \simeq \tilde{a}_n$. Strong hybridization and interconnection between the PD photon and exciton dispersions take place, so that the lower (upper) polariton dispersion branch n is exciton-like (photon-like) at $\tilde{a} \ll \tilde{a}_n$ and becomes photon-like (exciton-like) at $\tilde{a} \gg \tilde{a}_n$. According to figure 4, we classify the PD polariton spectrum in terms of the upper ($\tilde{\omega}^{\rm pol}_n = \tilde{\omega}^U_n > \tilde{\omega}_L = \sqrt{1 + \tilde{\omega}^2_{\rm p}}$) and lower ($\tilde{\omega}^{\rm pol}_n = \tilde{\omega}^L_n \leqslant \tilde{\omega}_T$) polariton branches. For the TM_1 polariton eigen-states, in both the strong and weak coupling regimes, one extra mode has a frequency $\tilde{\omega}^{\rm pol}_S = \tilde{\omega}^{\rm pol}_{n=0}$ in the optical 'stop band', $1 \leqslant \tilde{\omega}^{\rm pol}_S \leqslant \tilde{\omega}_L$. This is a well-known Fröhlich surface mode [10, 22], and its frequency $\tilde{\omega}^{\rm pol}_S \to [1 + \tilde{\omega}^2_{\rm p}/(1 + 2\tilde{\varepsilon})]^{1/2}$ when $\tilde{a} \to 0$.

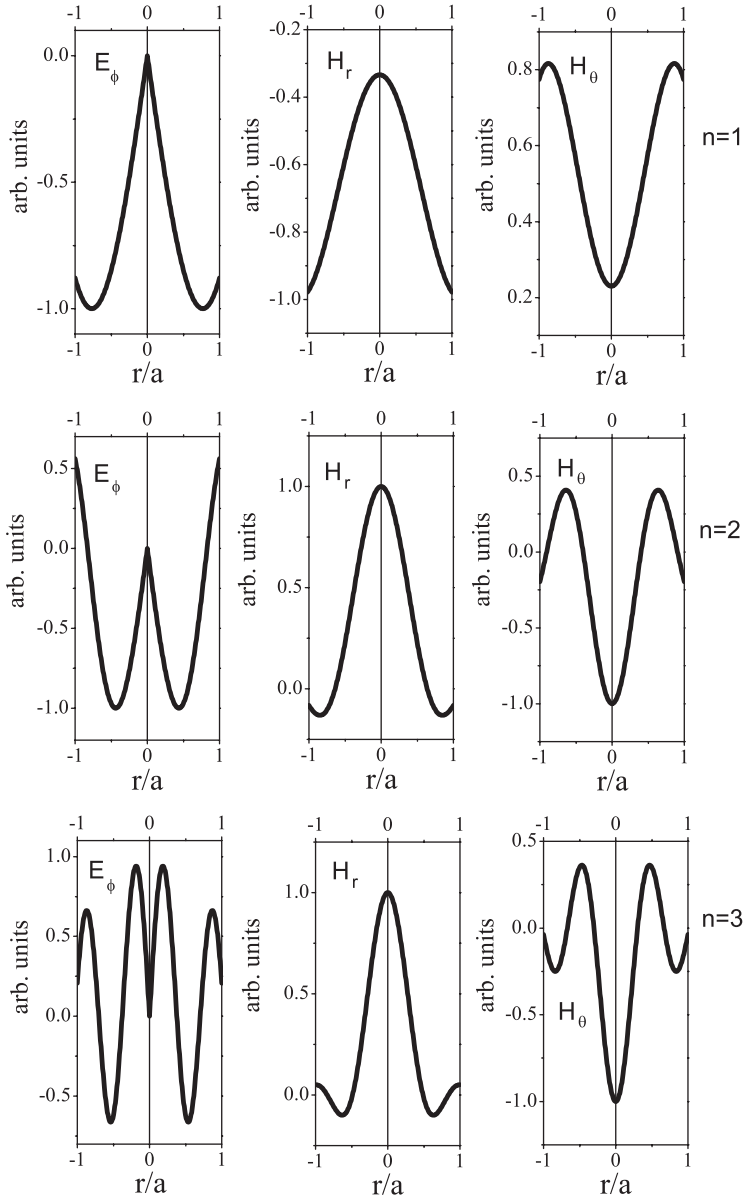

Figure 3. The eigen-fields of the photon-like polariton TE_1 mode (the weak coupling regime), for $n = 1$, 2 and 3. The spherical coordinates are given by $\{r, \phi, \theta\}$, where r is the radial distance from the centre of the PD and ϕ and θ are the polar angles. The PD parameters are the same as in figure 2.

While the polariton dispersion in bulk semiconductors, $\tilde{\omega}^{\rm pol}_{\rm bulk} = \tilde{\omega}^{\rm pol}_{\rm bulk}(k)$, deals with the dependence of the polariton frequency against the polariton wavevector $\mathbf{k}$ [8, 19, 20, 24], the PD polariton dispersion refers to the PD-radius dependence, $\omega^{\rm pol}_n = \omega^{\rm pol}_n(a)$. Similar to the former case, when for a given $\mathbf{k}$ only two initial eigenstates (photon $\mathbf{k}$ and exciton $\mathbf{k}$) couple each other, in the spherical PD of a given radius a only two energy states, ω^0_n and ω_T, interact resonantly

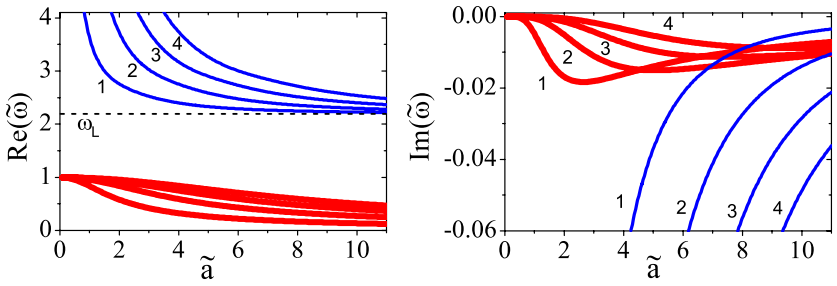

Figure 4. The PD polariton eigen-frequencies $\tilde{\omega} = \tilde{\omega}^{\rm pol}_{n=1,2,3\ldots}(\tilde{a})$ for the TE_1 mode in the strong coupling regime; $\tilde{\omega}_p = 1.95$ and $\tilde{\varepsilon} = 0.52$ (the parameters refer to dipole-active optical phonons in a vacuum-placed LiF sphere). The upper (lower) dispersion branches are depicted by thin blue (thick red) solid curves.

and independently of the other energy states. This can easily be illustrated by equations (5) and (6) where the energy number n appears on the right-hand-side of the equations and labels the pairs of the resonantly interacting PD states. If the maximum number of the energy states we examine is N, the factor N degeneracy should be attributed to the non-dispersive exciton state. In this case the resonant exciton–photon interaction removes the degeneracy of the initial exciton term even in the limit of weak exciton–photon coupling (see the right-hand-side plots in figure 2).

3. The radiative lifetime of PD polaritons and coherent excitons

In our model the incoherent damping rates due to phonon scattering, etc are neglected ($\gamma_x = 0$), but the eigenfrequencies given by the dispersion equations (3) and (4) are complex. This is due to the intrinsic escape of photons from the photonic dot. In this case $\mathrm{Im}\{\tilde{\omega}_n\} < 0$ and $\Gamma_n = -2\,\mathrm{Im}\{\tilde{\omega}_n\}$ is the width of the mode, or the inverse optical lifetime $\tau_n = 1/\Gamma_n$ [25]. In the previous section we have already discussed the numerical solution of the dispersion equations and now proceed to develop analytical approximations for the radiative lifetime. In particular, we consider the cases of small and large radius, $\tilde{a}$, for states with angular momentum $l = 1$, i.e. TE_1 and TM_1 modes.

For a small radius ($\tilde{a} \ll 1$) in both the weak and strong coupling limits, one has

$$\text{Photon-like/upper branch: } \Gamma_n^{\gamma,U} = 2B_n\omega_T/\tilde{a},$$

$$\text{Exciton-like/lower branch: } \Gamma_n^{x,L} = \begin{cases} \dfrac{2\tilde{\omega}_{\rm p}^2[(1+2\tilde{\varepsilon})+\tilde{\omega}_{\rm p}^2]^2(\tilde{\varepsilon})^{5/2}\tilde{a}^3\omega_T}{(1+2\tilde{\varepsilon})^2[(1+2\tilde{\varepsilon})^2+\tilde{\omega}_{\rm p}^2]} \\ \qquad \text{for } TM_1,\ n=0 \text{ (Fröhlich) mode}, \\ \dfrac{2\tilde{\omega}_{\rm p}^2(\tilde{\varepsilon})^{5/2}\tilde{a}^7\omega_T}{A^4} \\ \qquad \text{for } TM_1,\ n=1,2,3\ldots \text{ modes}, \\ \dfrac{2\tilde{\omega}_{\rm p}^2(\tilde{\varepsilon})^{3/2}\tilde{a}^5\omega_T}{A^4} \\ \qquad \text{for } TE_1,\ n=1,2,3\ldots \text{ modes}, \end{cases} \tag{8}$$

where $B_n = -\,\mathrm{Im}\{Z_n\} \simeq \sqrt{\tilde{\varepsilon}}$. $A = n\pi$ for TE_1 and $A = (n+1/2)\pi$ for TM_1 modes. Here $Z = Z_n$ is the single solution of equation:

$$Z = \arctan\left[\frac{Z\tilde{\varepsilon}}{\mathrm{i}Z\sqrt{\tilde{\varepsilon}}-1+\tilde{\varepsilon}}\right] + n\pi, \tag{9}$$

for the TE_1 modes, and

$$Z = \arctan\left\{\frac{-iZ[Z^2\tilde{\varepsilon} + (1 - iZ\sqrt{\tilde{\varepsilon}})(\tilde{\varepsilon} - 1)]}{Z^3\tilde{\varepsilon}\sqrt{\tilde{\varepsilon}} + (Z\sqrt{\tilde{\varepsilon}} + i)(1 - \tilde{\varepsilon})}\right\} + n\pi, \tag{10}$$

for the TM_1 modes. For small radius dots, equation (8) gives for the ground-state ($n = 0$) exciton-like/lower-branch TM_1 polaritons (Fröhlich mode) the well-known result, $\Gamma^{X,L}_{n=0} \propto \tilde{a}^3$ [12, 13, 26]. Usually, such a behaviour is interpreted in terms of the PD-size-dependent coherent optical volume: for very small $\tilde{a}$ the optically coherent area is given by the PD volume, i.e. is $\propto\tilde{a}^3$. With increasing $\tilde{a}$ towards $\tilde{a} \sim 1$, the volume-dependent PD oscillator strength saturates, approaching the strength of exciton–photon interaction in the (PD) bulk material. According to equation (8) for $n \geqslant 1$ one has $\Gamma^{X,L}_n(\tilde{a} \to 0) \propto \tilde{a}^7$ for the TM_1 modes and $\Gamma^{X,L}_n(\tilde{a} \to 0) \propto \tilde{a}^5$ for the TE_1 modes. Thus, for a small PD radius, $\Gamma^{X,L}_{n=0} \propto \tilde{a}^3$ absolutely dominates over $\Gamma^{X,L}_n$ associated with the energy modes $n > 0$.

For a large radius ($\tilde{a} \gg 1$) in the weak coupling regime one has:

$$\begin{aligned} &\text{Photon-like branch: } \Gamma^{\gamma}_n = 2C_n\omega_T/\tilde{a}, \\ &\text{Exciton-like branch: } \Gamma^{x}_n = \frac{2(A + \pi/2)^2\tilde{\omega}^2_{\mathrm{p}}\omega_T}{\sqrt{\tilde{\varepsilon}}\tilde{\omega}^4_L\tilde{a}^3}. \end{aligned} \tag{11}$$

Here $C_n = -\operatorname{Im}\{R_n\}$, $\tilde{\omega}_L = \sqrt{1 + \tilde{\omega}^2_{\mathrm{p}}}$ is the longitudinal frequency, and $R = R_n$ is the single solution of the equation:

$$R = \frac{1}{\tilde{\omega}_L}\arctan\left[\frac{R\tilde{\varepsilon}\tilde{\omega}_L}{iR\sqrt{\tilde{\varepsilon}}\tilde{\omega}^2_L - \tilde{\omega}^2_L + \tilde{\varepsilon}}\right] + n\pi, \tag{12}$$

for the TE_1 modes, and

$$R = \frac{1}{\tilde{\omega}_L}\arctan\left\{\frac{-iR\tilde{\omega}_L[R^2\tilde{\varepsilon}\tilde{\omega}^2_L + (1 - iR\sqrt{\tilde{\varepsilon}})(\tilde{\varepsilon} - \tilde{\omega}^2_L)]}{R^3\tilde{\varepsilon}\sqrt{\tilde{\varepsilon}}\tilde{\omega}^2_L + (R\sqrt{\tilde{\varepsilon}} + i)(\tilde{\omega}^2_L - \tilde{\varepsilon})}\right\} + n\pi, \tag{13}$$

for the TM_1 modes.

According to equation (11), $\Gamma^{x}_n(\tilde{a} \to \infty) \propto 1/\tilde{a}^3$ decays with increasing dot radius much more rapidly than $\Gamma^{\gamma}_n(\tilde{a} \to \infty) \propto 1/\tilde{a}$, i.e. at large $\tilde{a}$ one has $\Gamma^{x}_n/\Gamma^{\gamma}_n \ll 1$. The radiative lifetime for the photon-like polaritons at large radius, $\tau^{\gamma}_n = 1/\Gamma^{\gamma}_n = \tilde{a}/2C_n\omega_T$, is $2C_n$ times smaller than the time needed for the propagation of the light from the centre of the sphere to the surface, $\tau_{\mathrm{ball}} = \tilde{a}/\omega_T$. Usually $C_n \sim 1$, so that we interpret $\tau^{\gamma}_n(\tilde{a} \to \infty)$ in terms of the time needed for the ballistic escape of photon-like polaritons from the large radius PD sphere. A similar ballistic decay channel is absent for the exciton-like polaritons because in our model the exciton state is assumed to be without translational spatial dispersion, i.e. the excitons are 'mechanically' non-propagating modes.

In figure 5 we plot $\Gamma^{x,\gamma}_{n=0} = \Gamma^{x,\gamma}_{n=0}(\tilde{a})$, numerically calculated from the dispersion equation (4), for the case of weak PD-exciton–photon coupling. The behaviour of $\Gamma^{x,\gamma}_{n=0}$ in the limits of small and large PD radius is highlighted in figure 6, which demonstrates the very good agreement of the derived approximations (8) and (11) with direct numerical solution of the dispersion equations.

In the weak coupling limit, according to equations (8) and (11), the ratio between the radiative lifetimes of photon-like and exciton-like PD polaritons, associated with the energy level $n = 0$ (TM_1 Fröhlich mode), for a small radius is

$$\tau^{x}_0/\tau^{\gamma}_0 = \frac{B_0[(1 + 2\tilde{\varepsilon})^2 + \tilde{\omega}^2_{\mathrm{p}}]}{\tilde{\omega}^2_{\mathrm{p}}\left[1 + \tilde{\omega}^2_{\mathrm{p}}/(1 + 2\tilde{\varepsilon})\right]^2\tilde{\varepsilon}^{5/2}\tilde{a}^4}, \tag{14}$$

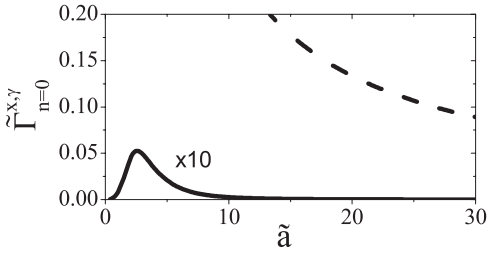

Figure 5. The dimensionless polariton radiative widths of the TM_1 mode, $\tilde{\Gamma}^x_{n=0} = \Gamma^x_{n=0}/\omega_T$ (solid curve) and $\tilde{\Gamma}^\gamma_{n=0} = \Gamma^\gamma_{n=0}/\omega_T$ (dashed curve), against the dimensionless PD radius $\tilde{a}$. The plot refers to the weak coupling limit of exciton–photon interaction in a cyanine dye J aggregate with $\tilde{\omega}_p = 0.09$ and $\tilde{\varepsilon} = 0.5$.

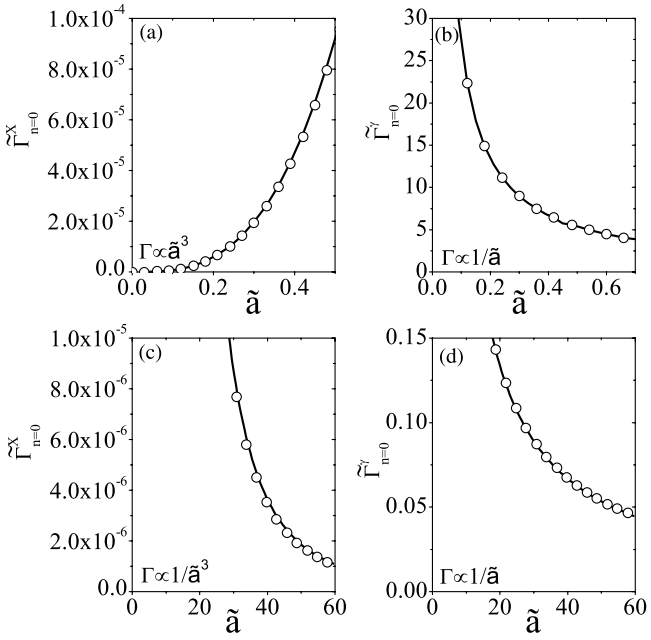

Figure 6. $\tilde{\Gamma}^{x,\gamma}_{n=0} = \Gamma^{x,\gamma}_{n=0}/\omega_T$ calculated with dispersion equation (4) (solid curve) and with approximations (8) and (11) (open circles): for $\tilde{a} \ll 1$, the exciton-like (a) and photon-like (b) polariton dispersion branches; and for $\tilde{a} \gg 1$, the exciton-like (c) and photon-like (d) dispersion branches. The PD parameters are the same as for figure 5.

and for a large radius:

$$\tau^x_n/\tau^\gamma_n = \frac{C_n\sqrt{\tilde{\varepsilon}}\tilde{\omega}_L^4\tilde{a}^2}{(A+\pi/2)^2\tilde{\omega}_p^2}, \tag{15}$$

for levels with the energy number n. Thus for both limits of the radius, the radiative lifetime of the exciton-like polaritons is greater than that of the photon-like polaritons.

Numerical evaluation of equations (3) and (4) shows that, for the weak coupling regime, the real parts of the frequencies of the photon- and exciton-like polariton branches approach asymptotic values, $\tilde{\omega}^\gamma_n \to 0$ and $\tilde{\omega}^x_n \to \tilde{\omega}_L$, as $\tilde{a} \to \infty$. In the strong coupling regime these asymptotic limits are swapped and become $\tilde{\omega}^U_n \to \tilde{\omega}_L$ and $\tilde{\omega}^L_n \to 0$, as $\tilde{a} \to \infty$. Thus in the

strong coupling regime and for $\tilde{a} \gg 1$ one has

$$\text{Upper branch: } \Gamma_n^U = \begin{cases} \dfrac{2(A-\pi/2)^2\tilde{\omega}_\mathrm{p}^2\omega_T}{\sqrt{\tilde{\varepsilon}}\tilde{\omega}_L^4\tilde{a}^3} & \text{for TM}_1 \text{ mode, } \tilde{\varepsilon} > 1, \\ \dfrac{2(A+\pi/2)^2\tilde{\omega}_\mathrm{p}^2\omega_T}{\sqrt{\tilde{\varepsilon}}\tilde{\omega}_L^4\tilde{a}^3} & \text{for all other modes,} \end{cases} \qquad (16)$$

$$\text{Lower branch: } \Gamma_n^L = 2C_n\omega_T/\tilde{a}.$$

In order to evaluate the total radiative lifetime τ_n, associated with a PD exciton, one needs to determine how the energy of incoming excitons is split between the upper and lower polariton dispersion branches. In our approach we assume a coherent distribution of the PD exciton in the energy state n between two relevant polariton branches, $(x, L), n$ and $(\gamma, U), n$. The above assumption is consistent with the kinetic population of the polariton states by exciton–exciton and exciton–phonon scattering, if $\tilde{a} \simeq \tilde{a}_n$.

The excitonic and photonic components of each polariton dispersion branch, X_n and Y_n, satisfy the polariton sum rule [8]:

$$\begin{aligned} X_n^{\gamma,U} + X_n^{x,L} &= 1, \qquad & Y_n^{\gamma,U} + Y_n^{x,L} &= 1, \\ X_n^{\gamma,U} + Y_n^{\gamma,U} &= 1, \qquad & X_n^{x,L} + Y_n^{x,L} &= 1. \end{aligned} \qquad (17)$$

The excitonic component is given by $X = W_\mathrm{exc}/W$, where W_exc is the energy density associated with the excitonic polarization, and W is the total electromagnetic energy density equal to [19, 24, 27]

$$W = \frac{\varepsilon_\mathrm{b}\varepsilon_0\,|\boldsymbol{E}|^2}{4} + \frac{\mu_0\,|\boldsymbol{H}|^2}{4} + \frac{1}{4\varepsilon_\mathrm{b}\varepsilon_0\omega_\mathrm{p}^2}(|\omega\boldsymbol{P}|^2 + \omega_T^2\,|\boldsymbol{P}|^2). \qquad (18)$$

Here $\boldsymbol{E}$ and $\boldsymbol{H}$ are electric and magnetic fields, and $\boldsymbol{P}$ is the excitonic polarization. A non-magnetic semiconductor with no excitonic dispersion (Frenkel excitons) is assumed. Equation (18) yields

$$W = \frac{1}{4}\varepsilon_\mathrm{b}\varepsilon_0\,|\boldsymbol{E}|^2\left[1 + \sqrt{\left(1+\frac{\tilde{\omega}_\mathrm{p}^2}{1-\tilde{\omega}^2}\right)\left(1+\frac{\tilde{\omega}_\mathrm{p}^2}{1-\tilde{\omega}^{*2}}\right)} + \frac{(\tilde{\omega}\tilde{\omega}^*+1)\tilde{\omega}_\mathrm{p}^2}{(1-\tilde{\omega}^2)(1-\tilde{\omega}^{*2})}\right]. \qquad (19)$$

The exciton part of the energy is $W_\mathrm{exc} = W - W_\mathrm{phot}$, and

$$X = \frac{W - W_\mathrm{phot}}{W}. \qquad (20)$$

Here the photon part of the energy, W_phot, is given by

$$W_\mathrm{phot} = W\Big|_{\tilde{\omega}_\mathrm{p}=0} = 2\frac{\varepsilon_0\varepsilon_\mathrm{b}\,|\boldsymbol{E}|^2}{4}. \qquad (21)$$

Note that equations (17)–(21) deal with intrinsically complex polariton frequencies $\tilde{\omega} = \tilde{\omega}_n$, due to a finite radiative lifetime of PD polaritons.

Within our picture of the coherent distribution of incoming PD excitons among the relevant polariton dispersion branches, the lifetime τ_n^X of level n is $\tau_n^X = 1/\Gamma_n^X$, where Γ_n^X is given by

$$\Gamma_n^X = X_n^{\gamma,U}\Gamma_n^{\gamma,U} + X_n^{x,L}\Gamma_n^{x,L}. \qquad (22)$$

In figure 7 we plot the dependence $\Gamma_n^X = \Gamma_n^X(\tilde{a})$ for $n = 0$, 1 and 2. The maximum values of Γ_n^X refer to the PD radius $2a \simeq 2a_n \simeq n\lambda/2$, where $\lambda = (2\pi c)/(\omega_T\sqrt{\varepsilon_\mathrm{b}})$ is the wavelength of the light field resonant with the exciton state. In this case, the photon spatial quasi-eigenharmonics $n\lambda/2$, which can be interpreted in terms of constructive interference giving the

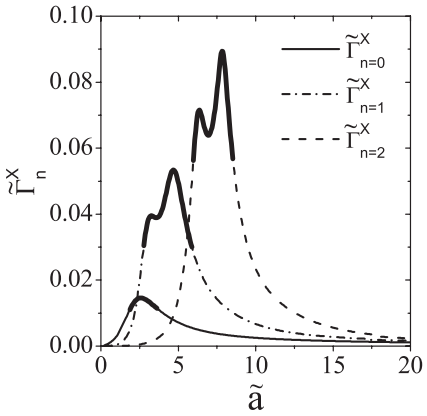

Figure 7. The exciton radiative width $\tilde{\Gamma}^X_{n=0,1,2} = \Gamma^X_{n=0,1,2}(\tilde{a})/\omega_T$ calculated with equation (22). The bold solid curves refer to the radius range near the resonant crossover between the PD photon and exciton dispersions, $\tilde{a} \simeq \tilde{a}_n$, where the coherent distribution of the exciton state between the polariton branches can occur. This simulation models a cyanine dye *J* aggregate with $\tilde{\omega}_p = 0.09$ and $\tilde{\varepsilon} = 0.5$.

standing light field pattern inside the spherical photonic dot, resonates with the exciton state. The first, less-developed maximum of $\Gamma^X_n(\tilde{a})$ is due to the TE_1 mode, while the second one, which occurs at larger values of $\tilde{a}$, is attributed to the TM_1 mode (see figure 7).

Our model is mostly relevant to $\tilde{a} \simeq \tilde{a}_n$. For either very small, $\tilde{a} \ll 1$, or very large, $\tilde{a} \gg 1$, PD radius, the excitonic radiative width Γ^X_n, evaluated by equation (22), is dominated by the photon-like polariton branches. In this case, the relevant polariton energies are rather far from the energy $\tilde{\omega}_T = 1$ of the optically undressed excitonic state, and, therefore, the coherent distribution of the incoming excitons among the polariton states is unlikely to occur. Nevertheless, to complete our description of Γ^X_n, below we examine analytic approximations of equation (22) for $\tilde{a} \ll 1$ and $\tilde{a} \gg 1$.

For $\tilde{a} \ll 1$, in both weak and strong limits of exciton–photon interaction, we obtain from equations (8), (20) and (22):

$$\begin{aligned} X^{\gamma,U}_n &= \frac{\tilde{\omega}_p^2(\tilde{a}^2 + B_n^2)\tilde{a}^2}{[(\tilde{a}^2 + B_n^2) - D_n^2]^2 + 4D_n^2B_n^2}, \qquad X^{x,L}_n = 1 - X^{\gamma,U}_n \simeq 1, \\ \Gamma^X_n &= X^{x,L}_n\Gamma^{x,L}_n + \frac{2B_n\omega_T\tilde{\omega}_p^2(\tilde{a}^2 + B_n^2)\tilde{a}}{[(\tilde{a}^2 + B_n^2) - D_n^2]^2 + 4D_n^2B_n^2} \simeq \frac{2\omega_T\tilde{\omega}_p^2B_n^3\tilde{a}}{(B_n^2 + D_n^2)^2}, \end{aligned} \tag{23}$$

where $D_n = \mathrm{Re}\{Z_n\}$ and Z_n is given by equations (9) and (10). Equation (23) shows that coherent distribution between the polariton branches results in the linear dependence $\Gamma^X_n \propto \tilde{a}$. This is due to the strongly dominant contribution to the optical decay from the photon-like/upper-branch polariton levels, i.e. in equation (22) one has $X^{\gamma,U}_n\Gamma^{\gamma,U}_n \gg X^{x,L}_n\Gamma^{x,L}_n$, if $\tilde{a} \ll 1$.

For $\tilde{a} \gg 1$ in the weak coupling regime, equations (11), (20) and (22) yield

$$\begin{aligned} X^{\gamma}_n &= \frac{\tilde{\omega}_p^2}{(1 + \tilde{\omega}_p^2)}, \qquad X^{x}_n = 1 - X^{\gamma}_n = \frac{1}{(1 + \tilde{\omega}_p^2)}, \\ \Gamma^X_n &= \frac{2C_n\omega_T\tilde{\omega}_p^2}{(1 + \tilde{\omega}_p^2)\tilde{a}} + \frac{2(A + \pi/2)^2\tilde{\omega}_p^2\omega_T}{\sqrt{\tilde{\varepsilon}}\tilde{\omega}_L^4(1 + \tilde{\omega}_p^2)\tilde{a}^3}. \end{aligned} \tag{24}$$

In a similar way, for $\tilde{a} \gg 1$ and the strong coupling regime, one derives from equations (16), (20) and (22):

$$X_n^U = \frac{1}{(1+\tilde{\omega}_\mathrm{p}^2)}, \qquad X_n^L = 1 - X_n^U = \frac{\tilde{\omega}_\mathrm{p}^2}{(1+\tilde{\omega}_\mathrm{p}^2)},$$
$$\Gamma_n^X = \frac{2C_n\omega_T\tilde{\omega}_\mathrm{p}^2}{(1+\tilde{\omega}_\mathrm{p}^2)\tilde{a}} + \frac{2\tilde{\omega}_\mathrm{p}^2\omega_T}{\sqrt{\tilde{\varepsilon}}\tilde{\omega}_L^4(1+\tilde{\omega}_\mathrm{p}^2)\tilde{a}^3} \begin{cases} (A-\pi/2)^2 & \text{for the TM}_1 \text{ mode, } \tilde{\varepsilon} > 1, \\ (A+\pi/2)^2 & \text{for all other modes.} \end{cases} \tag{25}$$

Thus for $\tilde{a} \to \infty$ equations (24) and (25) are approximated by the same formula:

$$\Gamma_n^X \simeq \frac{2C_n\omega_T\tilde{\omega}_\mathrm{p}^2}{(1+\tilde{\omega}_\mathrm{p}^2)\tilde{a}}. \tag{26}$$

Equation (26) yields $\tau_n^X \propto \tilde{a}$, which can be interpreted in terms of the ballistic escape ('optical evaporation') of optically dressed excitons from large-size spherical photonic dots. The ratio between radiative time $\tau_n^X = 1/\Gamma_n^X$ and the time for the propagation of the light from the centre of the sphere to the surface, τ_ball, is $\tau_n^X/\tau_\mathrm{ball} = 1/(\Gamma_n^X\tau_\mathrm{ball}) = (1+\tilde{\omega}_\mathrm{p}^2)/(2C_n\tilde{\omega}_\mathrm{p}^2)$. In this expression the term $\tilde{\omega}_\mathrm{p}^2/(1+\tilde{\omega}_\mathrm{p}^2)$ takes into account the excitonic component of the polariton branch with zero asymptotic frequency as $\tilde{a} \to \infty$ (photon-like branch for the weak interaction regime, lower-branch for the strong). For the weak coupling regime (e.g. for *J* aggregates with $\tilde{\omega}_\mathrm{p} = 0.09$) the exciton part is very small and $\tau_n^X/\tau_\mathrm{ball} \gg 1$. For the strong coupling regime, when $\tilde{\omega}_\mathrm{p} \simeq 1$, the excitonic component is of the order of unity so that $\tau_n^X/\tau_\mathrm{ball} \simeq 1/2C_n \sim 1$.

4. Transition between the strong and weak coupling regimes

According to the classification proposed in section 2, in photonic dots the weak coupling regime of exciton–photon interaction deals with photon-like and exciton-like polariton dispersions, $\omega_{i=1}^\mathrm{pol} \simeq \omega^\gamma(a)$ and $\omega_{i=2}^\mathrm{pol} \simeq \omega^x(a)$, while the strong coupling limit refers to the well-developed upper- and lower-branch polariton eigenfrequencies, $\omega_{i=1}^\mathrm{pol} = \omega^U(a)$ and $\omega_{i=2}^\mathrm{pol} = \omega^L(a)$. Within a completely coherent picture, one can easily control the transition between these two limits simply by changing ω_p, i.e. the oscillator strength of exciton–photon interaction, and keeping all other parameters unchanged. This intrinsic transition, which occurs at a critical value of ω_p, i.e. $\omega_\mathrm{p} = \omega_\mathrm{p}^\mathrm{cr}$, can be visualized as the intersection of two dispersion curves, $\omega_{i=1}^\mathrm{pol} = \omega_{i=1}^\mathrm{pol}(a)$ and $\omega_{i=2}^\mathrm{pol} = \omega_{i=2}^\mathrm{pol}(a)$, in a three-dimensional space $(a, \mathrm{Re}\{\omega^\mathrm{pol}\}, \mathrm{Im}\{\omega^\mathrm{pol}\})$. The topology of the polariton dispersion curves changes at $\omega_\mathrm{p} = \omega_\mathrm{p}^\mathrm{cr}$, so that for $\omega_\mathrm{p} \leqslant \omega_\mathrm{p}^\mathrm{cr}$ ($\omega_\mathrm{p} \geqslant \omega_\mathrm{p}^\mathrm{cr}$) one has the 'crossing' ('anti-crossing') behaviour of $\mathrm{Re}\{\omega_{i=1}^\mathrm{pol}\}$ and $\mathrm{Re}\{\omega_{i=2}^\mathrm{pol}\}$, i.e. the weak (strong) coupling regime. The transition is illustrated in figure 8.

The intersection point, which occurs at a critical PD radius, $a = a_n^\mathrm{cr} \simeq a_n$, is characterized by the degenerate roots, $\omega_{i=1}^\mathrm{pol} = \omega_{i=2}^\mathrm{pol}$. Thus, the criterion for the transition is given by

$$\mathrm{Re}\{\tilde{\omega}_n^{\gamma,U}\} = \mathrm{Re}\{\tilde{\omega}_n^{x,L}\},$$
$$\mathrm{Im}\{\tilde{\omega}_n^{\gamma,U}\} = \mathrm{Im}\{\tilde{\omega}_n^{x,L}\}. \tag{27}$$

For a given PD energy level *n*, equations (27) can also be interpreted as the relationship between two sets of the critical parameters: $(\tilde{a}_n^\mathrm{cr}, \tilde{\omega}_\mathrm{p}^\mathrm{cr})$ for the constant ratio of the background dielectric constants and $(\tilde{a}_n^\mathrm{cr}, \tilde{\varepsilon}^\mathrm{cr})$ for the constant oscillator strength of exciton–photon interaction. The latter set refers to the transition between two regimes, which is induced by changing $\tilde{\varepsilon}$. This case, illustrated in figure 9, can be realized experimentally by changing the background dielectric constant ε_d of the medium surrounding the PD, e.g. by applying an external mechanical pressure.

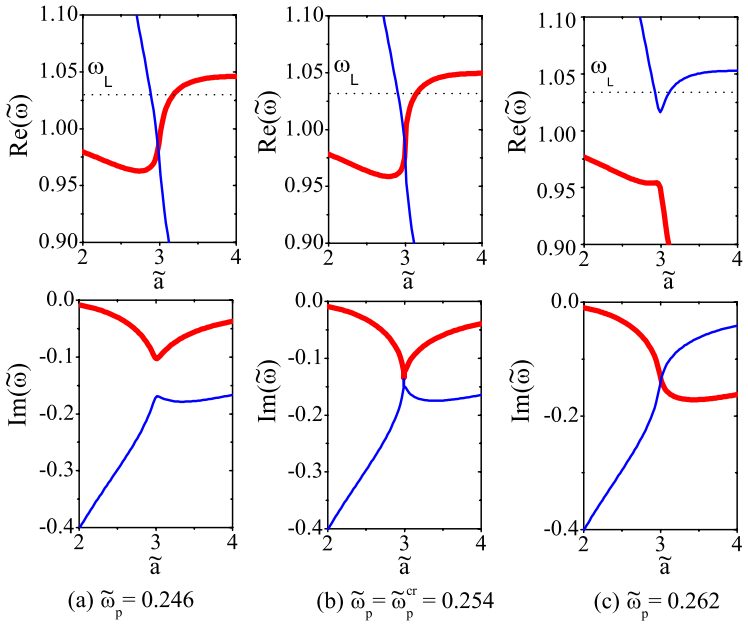

Figure 8. Transition between the weak and strong coupling limits for the TE_1 mode, $n = 1$ and $\tilde{\varepsilon} = 0.5$. The critical value of the oscillator strength is given by $\tilde{\omega}_p^{cr} = 0.254$; (a) weak coupling regime, $\tilde{\omega}_p < \tilde{\omega}_p^{cr}$, (b) $\tilde{\omega}_p = \tilde{\omega}_p^{cr}$ and (c) strong coupling regime, $\tilde{\omega}_p > \tilde{\omega}_p^{cr}$.

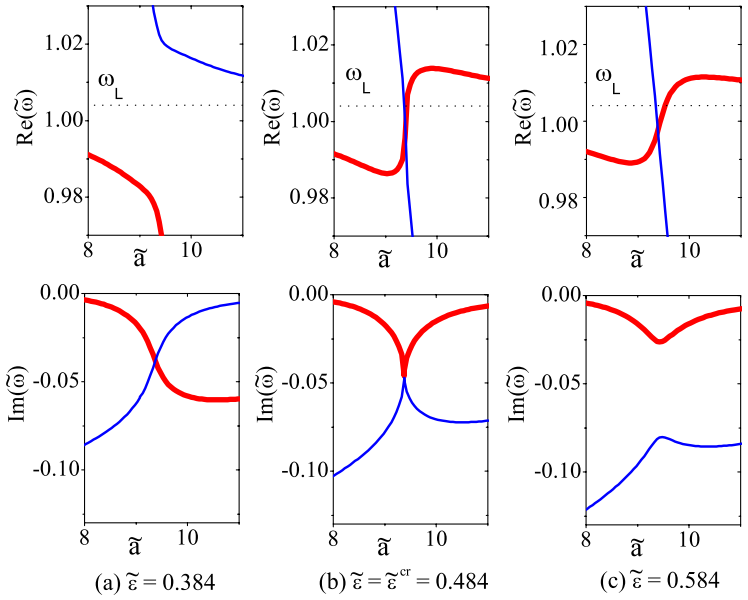

Figure 9. Transition between the weak and strong coupling regimes, induced by changing $\tilde{\varepsilon}$, for the TE_1 mode, $n = 3$ and $\tilde{\omega}_p = 0.09$. The critical value of the relative dielectric constant, $\tilde{\varepsilon} = \varepsilon_d/\varepsilon_b$, is given by $\tilde{\varepsilon}^{cr} = 0.484$; (a) strong coupling regime, $\tilde{\varepsilon} < \tilde{\varepsilon}^{cr}$, (b) $\tilde{\varepsilon} = \tilde{\varepsilon}^{cr}$ and (c) weak coupling regime, $\tilde{\varepsilon} > \tilde{\varepsilon}^{cr}$.

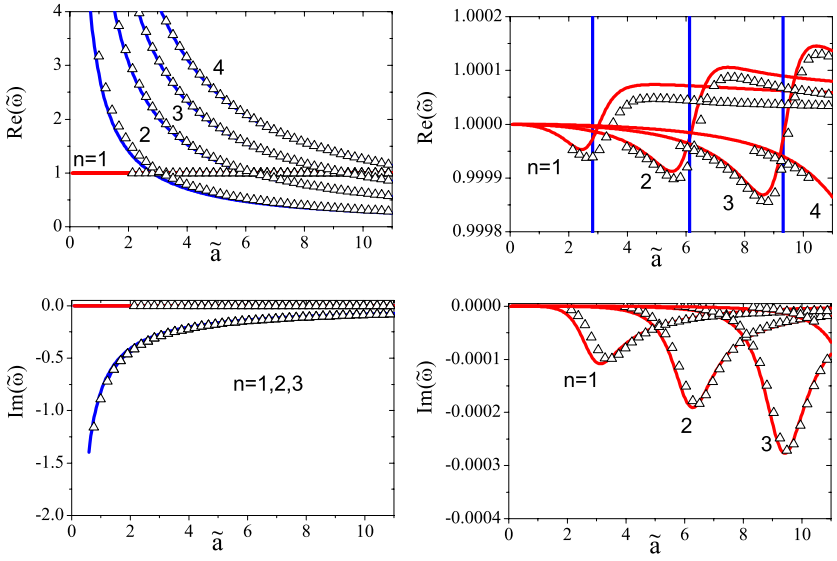

Figure 10. Approximation (triangle points) by the cubic equation (28) of the polariton dispersion curves (solid curves) calculated with the relationships (5) and (6). TE_1 mode, $\tilde{\varepsilon} = 0.5$ and $\tilde{\omega}_p = 0.01$.

Considering $\tilde{\omega}_p^2$ as a small dimensionless parameter, we approximate the dispersion equations (5) and (6) by the cubic equation:

$$\tilde{\omega}^3 - a_2\tilde{\omega}^2 - a_1\tilde{\omega} - a_0 = 0, \tag{28}$$

where

$$a_0 = -a_2 + \frac{i\tilde{\omega}_p^2\sqrt{\tilde{\varepsilon}}}{2\tilde{a}(\tilde{\varepsilon}-1)}, \qquad a_1 = 1 + \frac{\tilde{\omega}_p^2}{2}, \qquad \text{and}$$
$$a_2 = \begin{cases} \dfrac{1}{\tilde{a}}[\arctan(-i\sqrt{1/\tilde{\varepsilon}}) + n\pi] & \text{for } TM_1 \text{ modes,} \\ \dfrac{1}{\tilde{a}}[\arctan(-i\sqrt{\tilde{\varepsilon}}) + n\pi] & \text{for } TE_1 \text{ modes.} \end{cases} \tag{29}$$

In figure 10 we show that the cubic approximation (28) is very accurate for $\tilde{a} \simeq \tilde{a}_n$, i.e. where the transition between two coupling limits occurs. Two roots of equation (28) approximate $\tilde{\omega} = \tilde{\omega}_{i=1,2}^{pol}$, while the third one is unphysical because it has a negative real part. By applying approximation (28), we reduce the criterion (27) to the following analytic equation:

$$(\tfrac{1}{3}a_1 + \tfrac{1}{9}a_2^2)^3 - [\tfrac{1}{6}(a_1a_2 + 3a_0) + \tfrac{1}{27}a_2^3]^2 = 0. \tag{30}$$

Equation (30) allows us to readily calculate the relationships for the critical parameters, $\tilde{\omega}_p^{cr} = \tilde{\omega}_p^{cr}(\tilde{\varepsilon})$ and $\tilde{a}_n^{cr} = \tilde{a}_n^{cr}(\tilde{\varepsilon})$; $\tilde{\varepsilon}^{cr} = \tilde{\varepsilon}^{cr}(\tilde{\omega}_p)$ and $\tilde{a}_n^{cr} = \tilde{a}_n^{cr}(\tilde{\omega}_p)$ (see figure 11).

The transition between the weak and strong coupling regimes influences the radiative decay of coherent PD excitons. In figure 12 we plot the dependence $\widetilde{\Gamma}_n^X = \Gamma_n^X/\omega_T(\tilde{a})$ calculated with equation (22) for the constant Rabi frequency $\tilde{\omega}_p$ and for the dielectric permittivity $\tilde{\varepsilon}$ changing around its critical value $\tilde{\varepsilon}^{cr}$ (see also figure 9). According to the plot, a 'vertical-wedge' shape of $\widetilde{\Gamma}_n^X = \widetilde{\Gamma}_n^X(\tilde{a})$, which is accompanied by a jump of the derivative $d\widetilde{\Gamma}_n^X/d\tilde{a}$ at $\tilde{a} = \tilde{a}_n^{cr} \simeq \tilde{a}_n$, occurs for $\tilde{\varepsilon} = \tilde{\varepsilon}^{cr}$. This is illustrated by figure 13(a). In a similar way, the derivative $d\widetilde{\Gamma}_n^X/d\tilde{\varepsilon}$ changes its dependence against the PD radius $\tilde{a}$, with increasing $\tilde{\varepsilon}$ from $\tilde{\varepsilon} < \tilde{\varepsilon}^{cr}$ to $\tilde{\varepsilon} > \tilde{\varepsilon}^{cr}$, and

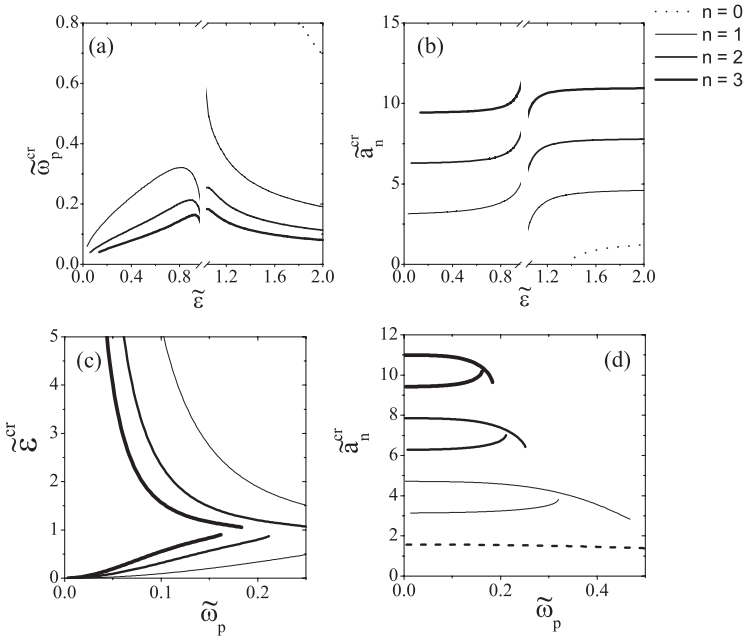

Figure 11. The dimensionless critical parameters evaluated with equation (30); (a) $\tilde{\omega}_{\rm p}^{\rm cr} = \tilde{\omega}_{\rm p}^{\rm cr}(\tilde{\varepsilon})$, (b) $\tilde{a}_n^{\rm cr} = \tilde{a}_n^{\rm cr}(\tilde{\varepsilon})$, (c) $\tilde{\varepsilon}^{\rm cr} = \tilde{\varepsilon}^{\rm cr}(\tilde{\omega}_{\rm p})$ and (d) $\tilde{a}_n^{\rm cr} = \tilde{a}_n^{\rm cr}(\tilde{\omega}_{\rm p})$.

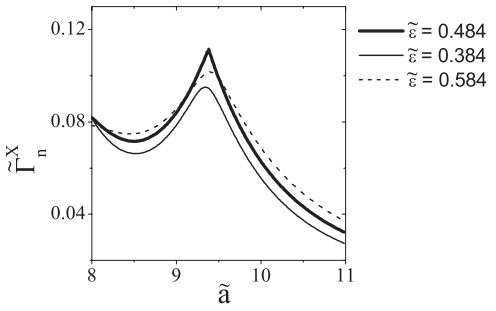

Figure 12. The radiative width of optically dressed PD excitons, associated with the energy state $n = 3$, against the dimensionless PD radius $\tilde{a}$. The contributions from both TE_1 and TM_1 are included, $\tilde{\omega}_{\rm p} = 0.09$ and $\tilde{\varepsilon}^{\rm cr} \simeq 0.484$.

undergoes a jump at $\tilde{a} = \tilde{a}_n^{\rm cr}$ for $\tilde{\varepsilon} = \tilde{\varepsilon}^{\rm cr}$ (see figure 13(b)). Thus the discontinuous behaviour of the derivatives of $\widetilde{\Gamma}_n^X$ at the critical values of the parameters is a direct manifestation of the transition between the two limits of exciton–photon coherent coupling in semiconductor photonic dots. Note that, as we have already discussed, equation (22) is mostly relevant to $\tilde{a} \simeq \tilde{a}_n \simeq \tilde{a}_n^{\rm cr}$, i.e. it is applicable to the above analysis.

High-precision modulation spectroscopy [28] is potentially applicable to visualize the transition between photon-like and exciton-like PD polaritons to the well-developed PD polariton states. In this case, the modulation of $\varepsilon_{\rm d}$, i.e. of $\tilde{\varepsilon}$, can be achieved by applying a time-dependent pressure [29] or electric field [30]. The PD radius modulation can probably be realized by the surface acoustic wave technique, which has recently been adapted to small spheres [31].

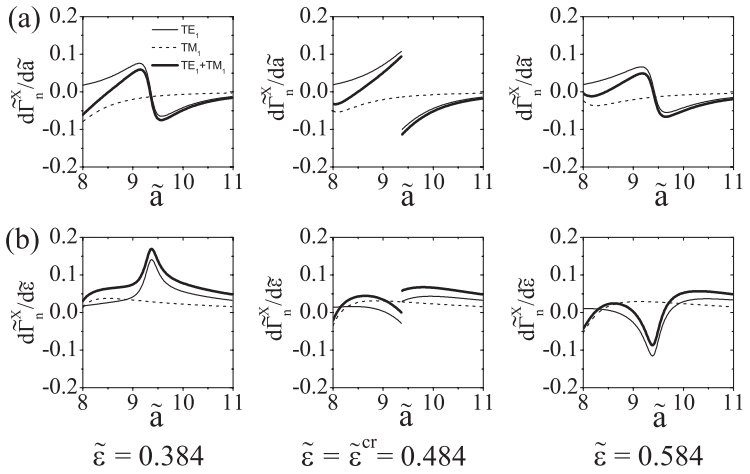

Figure 13. The derivatives (a) $d\widetilde{\Gamma}^X_{n=3}/d\tilde{a}$ and (b) $d\widetilde{\Gamma}^X_{n=3}/d\tilde{\varepsilon}$ versus the PD radius $\tilde{a}$. The parameters are the same as for figure 12. While both TE_1 and TM_1 modes contribute to $\widetilde{\Gamma}^X_{n=3}$, the critical value $\tilde{\varepsilon}^{cr} \simeq 0.484$ refers to the transition associated with the TE_1 mode.

5. Conclusions

In this paper we have developed polariton optics of dispersionless excitons in spherical photonic dots of the radius $a \sim \lambda$, where $\lambda = (2\pi c)/(\omega_T\sqrt{\varepsilon_b})$ is the wavelength of the light field resonant with the exciton state. The following conclusions summarize our results.

(i) The classification of the PD optical states is given in terms of either photon-like and exciton-like polaritons (the weak coupling regime) or upper- and lower-branch polaritons (the strong coupling regime), according to the dispersion relationship $\omega^{pol}_{i=1,2} = \omega^{pol}_{i=1,2}(a)$.

(ii) The radiative width Γ^X_n of excitons, coherently distributed between the PD polariton states, increases $\propto a^3$ with increasing small radius $a \ll \lambda$, reaches maximum at $2a = 2a_n \sim n\lambda/2$, and decays $\propto 1/a$ with further increase of the PD radius towards $a \gg a_n$. The maximum values of Γ^X_n ($n = 0, 1, 2, \ldots$) are attributed to the PD geometrical resonances, when the PD sphere resonates with $n\lambda/2$ photon harmonics.

(iii) The transition between the weak and strong coupling regimes of exciton–photon interaction in semiconductor PDs is described in terms of the topological transition ('crossing' against 'anti-crossing') between two polariton dispersion curves, $\omega^{pol}_{i=1}$ and $\omega^{pol}_{i=2}$, in a three-dimensional space (a, $\mathrm{Re}\{\omega^{pol}\}$, $\mathrm{Im}\{\omega^{pol}\}$). The transition is characterized by two sets of the critical parameters, (a^{cr}_n, ω^{cr}_p) or (a^{cr}_n, $\tilde{\varepsilon}^{cr}$).

(iv) The transition between two limits of the PD exciton–photon interaction results in discontinuous behaviour (jumps) of the derivatives $d\Gamma^X_n/da$ and $d\Gamma^X_n/d\tilde{\varepsilon}$ at critical points (a^{cr}_n, $\tilde{\varepsilon}^{cr}$). The use of modulation spectroscopy is proposed in order to visualize the above spectral jumps.

Acknowledgments

We appreciate valuable discussions with K Cho, V V Nikolaev, A Kavokin, N Le Thomas, M-E Pistol and U Woggon. N I Nikolaev gratefully acknowledges the financial support provided through the European Community's Human Potential Programme under

contract HPRN-CT-2002-00298, RTN 'Photon-Mediated Phenomena in Semiconductor Nanostructures'. A Smith acknowledges the support of the Engineering and Physical Sciences Research Council.

References

[1] Zhuk V, Regelman D V, Gershoni D, Bayer M, Reithmaier J P, Forchel A, Knipp P A and Reinecke T L 2002 *Phys. Rev.* B **66** 115302
[2] Dasbach G, Bayer M, Schwab M and Forchel A 2003 *Semicond. Sci. Technol.* **18** S339
[3] Nikolaev V V, Kaliteevski M A, Cassagne D, Albert J P and Sotomayor-Torres C M 2002 *Phys. Status Solidi* a **190** 199
[4] Artemyev M V and Woggon U 2000 *Appl. Phys. Lett.* **76** 1353
[5] Mie G 1908 *Ann. Phys.* **25** 377
[6] Stratton J A 1941 *Electromagnetic Theory* (New York: McGraw-Hill)
[7] Chew W C 1995 *Waves and Fields in Inhomogenous Media* (New York: IEEE)
[8] Hopfield J J 1958 *Phys. Rev.* **112** 1555
[9] Hopfield J J and Thomas D G 1963 *Phys. Rev.* **132** 563
[10] Fuchs R and Kliewer K L 1968 *J. Opt. Soc. Am.* **58** 319
[11] Ekimov A I, Onushchenko A A, Raikh M E and Efros Al L 1985 *Zh. Eksp. Teor. Fiz.* **90** 1795
Ekimov A I, Onushchenko A A, Raikh M E and Efros Al L 1986 *Sov. Phys.—JETP* **63** 1054 (Engl. Transl.)
[12] Hanamura E 1987 *Solid State Commun.* **62** 465
[13] Hanamura E 1988 *Phys. Rev.* B **37** 1273
[14] Ruppin R 1981 *J. Opt. Soc. Am.* **71** 755
[15] Goupalov S V 2003 *Phys. Rev.* B **68** 125311
[16] Ajiki H and Cho K 2000 *Phys. Rev.* B **62** 7402
[17] Ajiki H, Tsuji T, Kawano K and Cho K 2002 *Phys. Rev.* B **66** 245322
[18] Cho K 2003 *Optical Response of Nanostructures: Microscopic Nonlocal Theory* (Berlin: Springer)
[19] Tait W C 1971 *Phys. Rev.* B **5** 648
[20] Ivanov A L, Haug H and Keldysh L V 1998 *Phys. Rep.* **296** 237
[21] Agranovich V M, Litinskaia M and Lidzey D G 2003 *Phys. Rev.* B **67** 085311
[22] Ruppin R 1982 *Electromagnetic Surface Modes* ed A D Boardman (Chichester: Wiley) pp 345–98
[23] Jackson J D 1998 *Classical Electrodynamics* (New York: Wiley) p 431
[24] Born M and Huang K 1954 *Dynamical Theory of Crystal Lattices* (Oxford: Clarendon)
[25] Kliewer K L and Fuchs R 1966 *Phys. Rev.* **150** 573
[26] Itoh T, Furumiya M, Ikehara T and Gourdon C 1990 *Solid State Commun.* **73** 271
[27] Ruppin R 2002 *Phys. Lett.* A **299** 309
[28] Cardona M 1969 *Modulation Spectroscopy* (New York: Academic)
[29] Zhang J, Zhang H, Chen J, Deng Y, Hu C, An L, Yang F, Li G-H and Zheng H 2002 *J. Phys.: Condens. Matter* **14** 5349
[30] Fisher T A, Afshar A M, Whittaker D M, Skolnick M S, Roberts J S, Hill G and Pate M A 1995 *Phys. Rev.* B **51** 2600
[31] Yamanaka K, Cho H and Tsukahara Y 2000 *Appl. Phys. Lett.* **76** 2797